# Discrete Element Study of Aggregate Damage during Asphalt Compaction

Erik Olsson[1], Denis Jelagin[2], Manfred Partl[3]
（[1] KTH Royal Institute of Technology, Department of Civil and Architectural Engineering, Brinellvägen 23 SE-100 44 Stockholm Sweden, erolsson@kth.se）
（[2] KTH Royal Institute of Technology, Department of Civil and Architectural Engineering, Brinellvägen 23 SE-100 44 Stockholm Sweden, jelagin@kth.se）
（[3] Empa Swiss Federal Laboratories for Materials Science and Technology, Laboratory of Road Engineering, Überlandstrasse 129 CH-8600 Dübendorf ,Switzerland, Manfred.partl@empa.ch）

## ABSTRACT

Loads in asphalt are mainly transferred through contact between the stones and the interaction between the stones and the binder. That makes asphalt suitable for investigations using the Discrete Element Method (DEM). This study focuses on prediction of compactability and damage of the aggregates. Explicitly, the influence of different aggregate gradations, mixture temperatures and binder properties are studied. In the DEM simulations, aggregate fracture is handled by a recently developed method of incorporating particle fracture in DEM, based on previously performed fracture experiments on granite specimens. The binder phase is modeled by adding a surface layer around each DEM particle. This surface layer has the same thickness as the binder. The mechanical properties for the binder at different temperatures are taken from literature. This DEM approach has been used for studying the behavior of asphalt mixtures in the compaction flow test and during gyratory compaction. The results show that the proposed DEM approach is able to provide both qualitative and quantitatively responses in both cases and also provide predictions of aggregate damage. One large benefit with the modelling approach is that different binder quantities and properties could be studied without re-calibration of model parameters.

**Keywords**: Simulations, Discrete Element Method, Gradations, Binder properties, Mechanical Behaviour

## 1. INTRODUCTION

The Discrete Element Method (DEM) provides a promising analysis tool for studying the mechanical behavior of asphalt mixtures, e.g. [1,2]. As compared to the finite element method, DEM allows capturing explicitly the rearrangement of particles in the material as well as accounting for the effect of particle fracture. Thus, DEM is particularly advantageous for examining asphalt mixture behavior at large deformations situations, such as compaction.

This study presents a newly developed DEM-based approach to study the macroscopic behavior of asphalt mixtures during compaction. In order to obtain accurate simulation results, an accurate contact law is essential, which provides the normal and shear forces on the aggregates. Based on the experimental results obtained in a previous study [3] together with results for viscoelastic contacts in the literature [4], new contact and failure laws for stones are developed and incorporated into the DEM model. Here, the basic concepts of this model are presented and discussed. The new DEM-based approach is used to model asphalt mixture behavior during a compaction flow test [2,5] and gyratory compaction. The ability of the model to capture the influence of mixture parameters on the compactability and the eventual stone

damage during compaction is examined. In particular, using a model with aggregates surrounded by a binder phase allows accounting for variations in mechanical and volumetric binder characteristics without any re-calibration of binder properties.

## 2. SIMULATION MODEL

### 2.1 Discrete Element Method

In the Discrete Element Method (DEM), which was invented by Cundall and Strack [6], each single particle is modelled as one object and the local contact forces acting between the objects determines the behaviour of the system. Hence, accurate models for the contact forces are of critical importance, as discussed below.

DEM is a time-stepping algorithm and in each time step $\Delta t$, the contact forces are calculated from the positions of the particles at the previous time step. To determine the positions at the next time step, Newton's second law for each particle is integrated explicitly. Due to the explicit nature of the algorithm, time steps cannot be made too large in order to have a numerically stable solution. In order to have a feasible large time step, mass scaling is applied which should not affect the response under quasi-static conditions [7] and is used in our study. The DEM simulations are implemented in an in-house software written in C++. More details can be found in [8,9].

### 2.2 Contact Model

The contact laws which provide the normal contact force *F* as function of the penetration *h* and the tangential contact force *T* as function of tangential displacement *s*, is of utmost importance for getting reliable predictions from the DEM simulations. For asphalt materials, one important issue is the large difference in forces for small and large penetrations.

For small penetrations, only the binder phase surrounding the particles comes into contact and "soft" viscoelastic behaviour is seen. The thickness $t_{BP}$ of this binder phase is assumed the same for all DEM particles. This binder phase includes both the asphalt binder and the fine stone particles that are too small to be included in the DEM simulations. When the penetration is larger than the thickness of the binder phase layer, the stones themselves start to deform and the contact gets much stiffer.

A visualization of this contact model is presented in FIGURE 1 (a). When the penetration is less than $2t_{PB}$, it is assumed that only the binder affects the contact behavior and the contact force can be calculated with a viscoelastic model using an incompressible binder material. This force is denoted $F_{binder}$. For implementation reasons, the behavior in shear of the binder material is described by a generalized Maxwell model and the expression for the relaxation modulus reads

$$G(t) = G_0\left[1 - \sum_{i=1}^{N} \alpha_i(1 - \exp(-t/\tau_i))\right] \quad (1)$$

where $G_0$, $\alpha_i$ and $\tau_i$ are material parameters for the binder phase. The contact force is then calculated using an incremental form of the solution presented by Lee and Radok [4]. The implementation of this part of the contact model is left out in this paper for brevity but will be presented and analyzed in an upcoming paper.

A last important part of the binder contact model is cohesion as indicated by the fracture force $F_{min}$ in FIGURE 1 (b). This bonding force is calculated using JKR theory [10] by

specifying the energy for separating the contacting surfaces. A value of $0.01\,\mathrm{J/mm^2}$ has been used here.

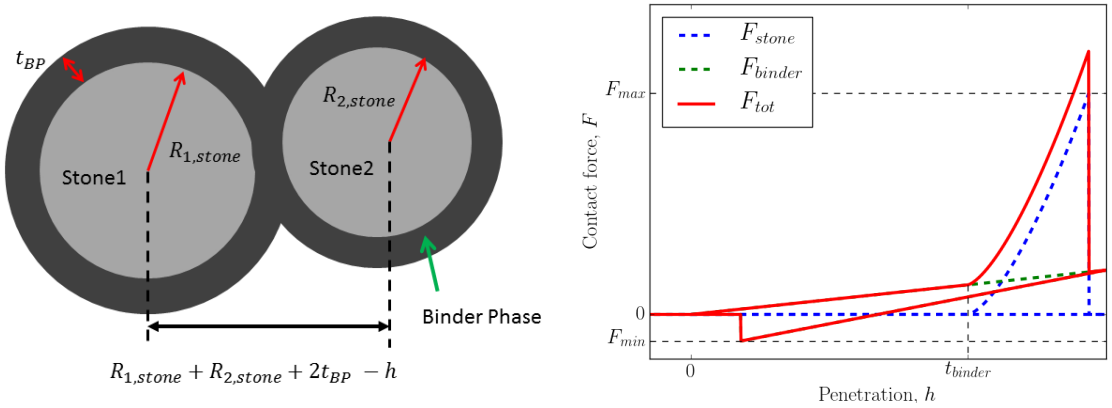


FIGURE 1: (a) Visualization of two aggregates, at presense of binder phase, in contact. (b) A sketch of the contact force as function of penetration between the particles.

When the penetration has exceeded $2t_{PB}$, the deformation of the stones themselves starts and a force $F_{stone}$ is added to the total force. This force is calculated using elastic contact theory by Hertz [11] knowing that an elastic behavior is a good approximation for stone contact in the normal direction [3]. The total normal contact force is thus given by

$$F_{tot}(h) = F_{binder}(h) + \frac{4}{3} E_0 \sqrt{R_{0,stone}} (h - 2t_{PB})^{3/2} H(h - 2t_{PB}) \tag{2}$$

Where $E_0$ is the reduced Young's modulus for the two contacting particles which for equal materials becomes $E/2/(1-\nu^2)$ with $\nu$ being the Poisson's ratio. $H(h-2t_{PB})$ is the Heaviside step function giving forces between the stones only when the penetration is larger than $2t_{PB}$. $R_{0,stone}$ is the effective contact radius for the stone contact defined as

$$\frac{1}{R_{0,stone}} = \frac{1}{R_{1,stone}} + \frac{1}{R_{2,stone}} \tag{3}$$

If the stone contact force, i.e. the second term in Eq. (2), exceeds a critical force $F_{max}$, the stone fractures and the technique for incorporating fracture of DEM particles presented in [12] is utilized. It is important to note that if the penetration is smaller than $2t_{BP}$, the stone will not fracture as the stone itself is not subjected to contact forces. A sketch of this normal force model is presented in FIGURE 1(b) where the magnitude of the binder force has been exaggerated for visualization purposes. At stone fracture, the stone loses its stiffness depending on the other contact forces acting on the particle. More details of the stiffness reduction is found in [12].

The tangential contact force as function of tangential displacement, $T(s)$, which acts between the particles and between particles and walls, is also important to consider as this force restrict the densification of the sample. However, tangential contact problems are much more difficult to analyze analytically than normal contact problems and thus more simplified models are needed. When only the binder force is active, the contact is assumed to be in a stick condition with no slip between the contact surfaces. Hence, a model based on a linear relationship between $T$ and $s$ is assumed but modified to account for the viscoelastic material behavior. The tangential stiffness is calculated from the binder properties according to [13] where the stiffness is proportional to the contact area. When the penetration is larger than $2t_{PB}$, a stick-slip frictional force is added, in the same way as for the normal force in Eq (2), assuming a coulomb friction coefficient of $\mu = 0.7$.

## 3. SIMULATION RESULTS

### 3.1 Numerical study

Two different aggregate gradations denoted AC11 and SMA11 are studied. The specified particle size distributions are presented in FIGURE 2 (a). In order to simulate a reasonable low number of particles, the fine particles smaller than 2 mm are discarded in the simulations and included implicitly in the simulation by the thickness and properties of the binder phase. All aggregates are assumed to be a spherical stone surrounded by a spherical binder shell with a thickness calculated to provide the simulated binder content.

Using a particle size distribution based on the weight-percent passing a sieve is unpractical for DEM. Hence, distributions based on the number of particles passing are constructed instead. This is performed by fitting the mean values, shown in FIGURE 2 (a), to a truncated normal distribution and then calculating the number percent of passing. This distribution is shown in FIGURE 2 (b).

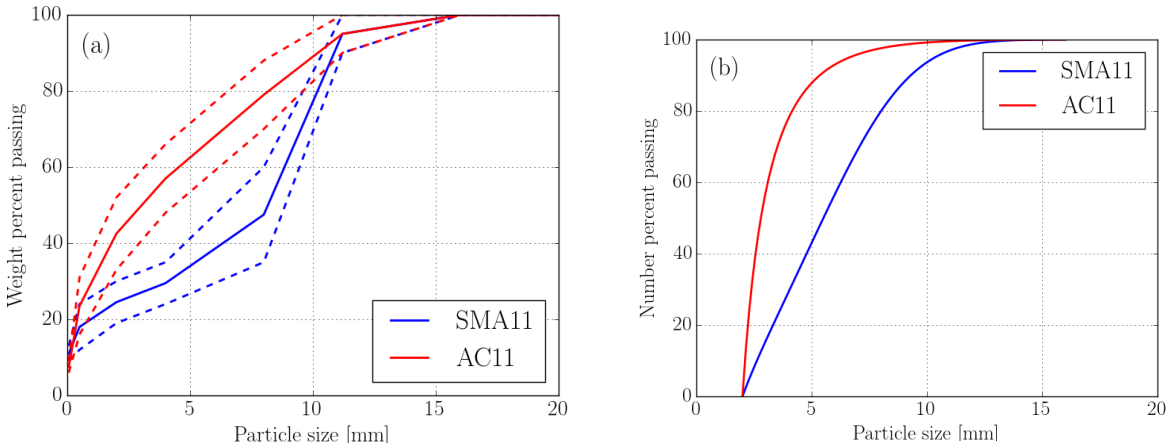


FIGURE 2: (a) The particle size distributions used presented as weight percent cumulative density function. The dashed lines show the limits and the solid line the mean used for generating the particles. (b) The same distributions presented in terms of number of particles.

The aggregates are assumed to be elastic with contact behavior as stated in Section 2.2. The Young's modulus and the Poisson's ratio are taken from the experimental results in [3] with values $E = 74$ GPa and $\nu = 0.15$. For the aggregate fracture model, each aggregate is assigned its own fracture strength $\sigma_F$ which is Weibull distributed according to the following cumulative density function $F$

$$F = 1 - \exp\left[-\left(\frac{\sigma_F}{\sigma_0}\right)^m \frac{V}{V_{ref}}\right] \tag{4}$$

where $\sigma_0$ and $m$ are material parameters determined in [3] to be. $\sigma_0 = 386.5$ MPa and $k = 3.87$. $V$ is a scaling volume for the spheres in the DEM model taken to be the particle radius cubed and $V_{eff}$ is a scaling effective volume of 244 mm$^3$.

The mechanical behavior of the binder phase is defined in Eq. (1), and suitable material data is found in [14]. The material data presented therein assumes a Burgers model with the drawback that the DEM particles will have zero modulus at infinite time. This issue has been solved by multiplying the relaxation parameters $\alpha_i$ with the amount of fine particles in the binder

phase. The used parameters for the generalized Maxwell model are presented in TABLE 1 for different temperatures.

TABLE 1: Material properties for the binder for the two different investigated temperatures. The data is taken from [14] and in the simulations, $\alpha_1$ and $\alpha_2$ needs to be multiplied with the volume fraction of binder in the binder phase layer.

| $T$ [°C] | $G_0$ [MPa] | $\alpha_1$ [-] | $\tau_1$ [s] | $\alpha_1$[-] | $\tau_2$ [s] |
|---|---|---|---|---|---|
| **110** | 17.74 | 0.684 | 0.0703 | 0.316 | 64.223 |
| **150** | 6.65 | 0.513 | 0.0948 | 0.487 | 105.9 |

### 3.2 Simulation of Particle flow Experiments

The first type of experiments that is simulated is the Compaction Flow Test presented in [5]. In these experiments, a container is filled with asphalt material having a volume of 150x100x100 $mm^3$. On one side of the container, a loading strip, with dimensions 50x100 $mm^2$ is moved downwards vertically to apply the loading. This is performed using controlled displacement with a velocity of 15 mm/min.

The simulation starts by generating a random "gas" of particles with a packing density of 30 %: In a second step, the packing is generated by applying a gravitational field to the particles. After the kinetic energy has decreased below a threshold value, the sample is considered in rest and the flow test begins. During the flow test, the force on the loading strip is monitored continuously together with the positions of the particles. The force divided by the area of the strip is presented in FIGURE 3 (a) as function of the displacement divided by the height of the particle bed. As expected, the simulated response is significantly weaker than the experimental results in [5] due to the much higher binder content assumed in the simulations. The noisy response in the simulations could be explained that only large aggregates are simulated. The uplift, which is defined as the increase of the mean of the 10 highest material points in the container is presented in FIGURE 3 (b). Initially, a compression of the sample is seen but eventually an uplift up to 5 mm occurs. This uplift increases with sample stiffness, i.e. with decreasing temperature and binder content, as expected. Also here, the response is a bit noisy which is due to the fact that the movement of a single particle has a large influence on the uplift, as defined here.

### 3.3 Simulation of Gyratory Compactor Experiments

The gyratory compactor simulations are initiated in the same way as for the particle flow test. After the particles have settled, a plate that is inclined with 1° is placed on the top of the particles. On that plate, a pressure of 600 kPa is applied by increasing the pressure linearly during one second. When the pressure is fully applied, the gyration starts by imposing a controlled rotation of the plate with a velocity of 0.5 revolutions per second. During gyration, the packing density is monitored continuously and is presented in the form of air void decrease in FIGURE 4 (a). A relative measure is chosen because the thick layer of binder and fine stone particle that surrounds each modelled particle becomes too compliant at high packing densities. This occurs because the hydrostatic pressure in the binder at high densities is not accounted for and therefore leads to an overestimated compressibility. The overestimated compressibility in the beginning is due to the fact that the binder material is distributed as a spherical shell around each stone and the first few gyrations have to level this layer.

The number of fractured particles is presented in FIGURE 4 (b) for different mixture temperatures, gradations and binder thicknesses. It is evident that fracture of the particles is very rare since only 0-4 out of 5000 particles fracture during the process. It is also seen that decreasing the binder temperature leads to a stiffer response and more frequent damage of the aggregates with increasing contact forces.

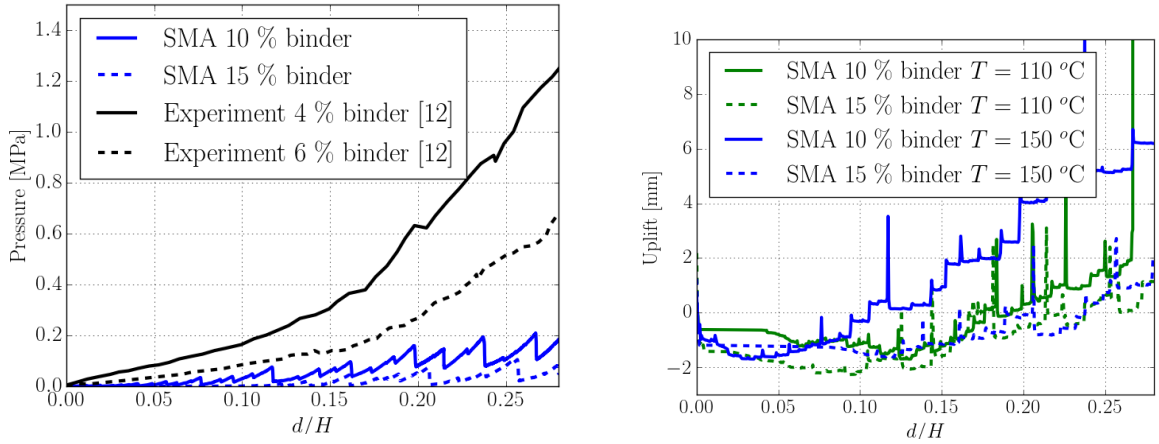


FIGURE 3: (a) Force displacement relationship at the flow test for SMA gradations at 150 °C. (b) The simulated uplift during the test.

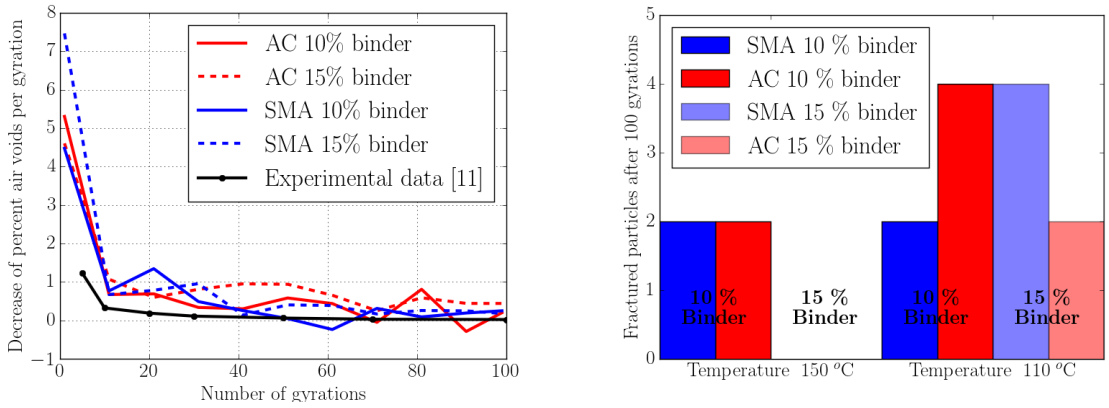


FIGURE 4: (a) Simulated air void change per gyration for a mixture at 150 °C. (b) The number of fractured particles for all studied configurations.

## 4. CONCLUSIONS

Using a DEM model where the asphalt is modelled as stones with a surrounding binder layer is concluded to be beneficial as different binder contents and binder types can be accounted for easily without re-calibrating contact law parameters. This has been demonstrated by providing adequate predictions for two different mechanical tests on asphalt mixtures. The DEM model also provides insights that are difficult to investigate experimentally, for instance aggregate damage. However, for qualitative predictions of air voids, further investigations are needed on the smallest size of aggregates that needs to be included in the model.

## REFERENCES


[1] Collop AC, McDowell GR, Lee YW. Modelling dilation in an idealised asphalt mixture using discrete element modelling. Granul Matter 2006;8:175–84.

[2] Ghafoori Roozbahany E, Partl MN. A new test to study the flow of mixtures at early stages of compaction. Mater Struct 2016;49:3547–58.

[3] Celma Cervera C, Jelagin D, Partl MN, Larsson P-L. Contact-induced deformation and damage of rocks used in pavement materials. Mater Des 2017;133:255–65.

[4] Lee EH, Radok JRM. The Contact Problem for Viscoelastic Bodies. J Appl Mech 1960;27:438.

[5] Ehsan Ghafoori Roozbahany, Manfred N.Partl, Alvaro Guarin. Particle flow during compaction of asphalt model materials. Constr Build Mater 2015;100:273–84.

[6] Cundall PA, Strack ODL. A discrete numerical model for granular assemblies. Géotechnique 1979;29:47–65.

[7] C. Thornton; S.J. Antony. Quasi–static deformation of particulate media. Philos Trans R Soc London A Math Phys Eng Sci 1998;356.

[8] Olsson E, Larsson P-L. On the effect of particle size distribution in cold powder compaction. J Appl Mech Trans ASME 2012;79.

[9] Olsson E, Larsson P-L. A numerical analysis of cold powder compaction based on micromechanical experiments. Powder Technol 2013;243.

[10] Johnson KL, Kendall K, Roberts AD, Johnsont KL. Surface Energy and the Contact of Elastic Solids. Source Proc R Soc London Ser A, Math Phys Sci 1971;324:301–13.

[11] Hertz H. Über die Berührung fester elastischer Körper. J Für Die Reine Und Angew Math 1882.

[12] Olsson E, Larsson P-L. Micromechanical investigation of the fracture behavior of powder materials. Powder Technol 2015;286.

[13] Olsson E, Larsson P-L. On the tangential contact behavior at elastic-plastic spherical contact problems. Wear 2014;319.

[14] Chen J, Huang B, Chen F, Shu X. Road Materials and Pavement Design Application of discrete element method to Superpave gyratory compaction Application of discrete element method to Superpave gyratory compaction. Road Mater Pavement Des 2012;13:480–500.